Energy Engineering

Tech Science Press

DOI: 10.32604/ee.2025.059651

ARTICLE

A Novel Control Strategy Based on π-VSG for Inter-Face Converter in Hybrid Microgrid

Kai Shi and Dongyang Yang*

Department of Electrical Engineering, Jiangsu University, Zhenjiang, 21200, China

*Corresponding Author: Dongyang Yang. Email: 2212207020@stmail.ujs.edu.cn

Received: 14 October 2024 Accepted: 19 December 2024 Published: 31 January 2025

ABSTRACT

The rapid development of new energy power generation technology and the transformation of power electronics in the core equipment of source-grid-load drives the power system towards the "double-high" development pattern of "high proportion of renewable energy" and "high proportion of power electronic equipment". To enhance the transient performance of AC/DC hybrid microgrid (HMG) in the context of "double-high," a π type virtual synchronous generator (π-VSG) control strategy is applied to bidirectional interface converter (BIC) to address the issues of lacking inertia and poor disturbance immunity caused by the high penetration rate of power electronic equipment and new energy. Firstly, the virtual synchronous generator mechanical motion equations and virtual capacitance equations are used to introduce the virtual inertia control equations that consider the transient performance of HMG; based on the equations, the π-type equivalent control model of the BIC is established. Next, the inertia power is actively transferred through the BIC according to the load fluctuation to compensate for the system's inertia deficit. Secondly, the π-VSG control utilizes small-signal analysis to investigate how the fundamental parameters affect the overall stability of the HMG and incorporates power step response curves to reveal the relationship between the control's virtual parameters and transient performance. Finally, the PSCAD/EMTDC simulation results show that the π-VSG control effectively improves the immunity of AC frequency and DC voltage in the HMG system under the load fluctuation condition, increases the stability of the HMG system and satisfies the power-sharing control objective between the AC and DC subgrids.

KEYWORDS

Hybrid AC/DC microgrid; electromotive force of DC motor; interface converter; virtual synchronous generator control

Glossary/Nomenclature/Abbreviations

BIC	Bidirectional interface converter
G-DCEMF	Generalized DC Electromotive Force
HMG	Hybrid microgrid
MG	Microgrid
PLL	Phase-locked loop
SPWM	Sine pulse width modulation
π-VSG	π type virtual synchronous generator

1 Introduction

The power system is establishing the "double high" development trend of "high proportion of renewable energy" and "high proportion of power electronic equipment" as a result of the growth of new energy generation and the evolution of "power electronics" of energy conversion equipment [1]. The use of HMG to address the issue of distributed energy consumption and absorption has grown in popularity to optimize the benefits of distributed power generation. HMG not only reduces the number of energy conversion devices but also has more flexibility than single-system MGs, which can be adapted to the actual needs and is an essential means to improve the utilization of resources in the context of "double-high" [2,3].

Many scholars have made significant contributions to the research of hybrid AC-DC microgrids. For example, literature [4] proposed a planning model to solve the optimal sizing problem of hybrid AC/DC microgrids by a novel GA/AC OPF algorithm, which provides a basis for designing bidirectional interface converters. In addition, research on toughness-driven modelling, operation, and evaluation of hybrid AC/DC microgrids is also of great significance, as it can help to cope better with extreme events and improve the toughness of microgrids [5]. In the HMG system, BIC coordinates the power between MGs, so the study and control of BIC is critical [6,7]. A new active sharing control based on droop control has been proposed to simulate the droop characteristics of a traditional synchronous generator, aiming to realize the power allocation and voltage and frequency regulation functions of the MG [8]. A normalized bidirectional droop control approach was presented for the power-sharing problem in HMGs. This method calculates the transmitted power flow by comparing the two normalized values [9,10]. A hierarchical control strategy for BICs is presented in the literature [11]. This strategy may maximize power interchange between the distribution grid and the MG while limiting the voltage variation brought on by droop control to a particular degree. However, the traditional droop control strategy can no longer actively provide inertia support for the system as distributed power sources become more prevalent in MGs. As a result, the dynamic characteristics of frequency and voltage deteriorate, endangering the stability of the HMG system and failing to fully utilize the potential of BIC to enhance the stability of the HMG system [12,13].

To solve the lack of inertia problem, the virtual synchronous generator (VSG) concept was developed [14]. The VSG technique gives inertia to the power electronic converter by simulating the equations of motion of a traditional synchronous generator's rotor to enhance the system's stability. Some scholars have used VSG control as the primary control scheme to improve the frequency transient performance. Usually, VSG control is employed to provide inertia for the AC bus frequency [15]. However, since the traditional VSG technique cannot realize the bidirectional flow of power, literature [16] also proposes an improved VSG control strategy for BICs, which establishes the relationship between VSG active power, voltage, and frequency. The previously mentioned control system disregards the dynamic properties of the DC voltage and only offers inertial support for the AC frequency. The BIC control must consider the stability of both the DC and AC sides to stabilize the MG system. A DC virtual voltage control approach based on VSG control was described in the literature [17] to support the DC bus voltage inertia and realize a bidirectional energy flow during rapid changes in load. However, the previously mentioned control approach aims to enhance one side of the converter's transient performance by providing a steady source on the other side. Literature [18] proposes a virtual inertia control approach for BIC to limit the power transfer of BIC during the dynamic process, which can restrict the drastic fluctuations to one side of the subgrid, but it cannot play the role of inertia support for the opposite side of the MG. Literature [19] proposes an integrated inertia control approach to improve the dynamic characteristics of HMGs. Still, it relies too much on communication to realize decentralized control and needs to clarify the magnitude of inertia support between the two subgrids. In terms of improving the dynamic response of the BIC through virtual inertia parameters, in the literature [20], the traditional DC electric potential equation is generalized. In contrast, the dynamic response of the BIC is improved by adding a virtual inductor to provide inertia for the system. However, this approach is a current-based control and cannot provide sufficient voltage and frequency support to the HMG during islanding operation.

In conclusion, the control requirements for BICs face many new challenges. Table 1 lists the current mainstream control strategies for BICs. In view of the shortcomings of the above studies, this paper considers the inertia demand on both sides of the AC and DC and adopts π-VSG control to provide voltage and frequency support for the AC and DC buses and inertia for the AC and DC subgrids.

Table 1: Comparison of research methods

Analysis and research	Advantage	Disadvantage	Ref.
Droop control	1. Simple and easy to control	1. Lack of inertia support capacity 2. Excessive change and volatility	[9,10]
Traditional VSG control	1. Proven technology for a wide range of applications 2. Provide frequency support	1. Unable to realize the bidirectional flow of power	[14,15]
An improved VSG control strategy for BIC	1. Realize the bidirectional flow of power	1. Consider only a single subgrid inertia improvement	[16]
Virtual inertia control	1. Improve the dynamic characteristics of HMGs	1. Unclear magnitude of inertial support between two side subgrids	[18,19]
G-DCEMF control	1. Optimized power response of BIC 2. Suppressed the impact of fluctuations in one side of the subgrid on neighboring subgrid	1. Current-based control is unable to provide voltage and frequency support for the system	[20]

To address the bidirectional power transfer requirements, inertia deficit, and stability problems of HMGs, this paper improves the electric potential equation of a traditional DC motor and realizes power sharing and distribution using virtual resistors. For BIC, a π-VSG control is suggested. Inertia for both AC and DC subgrids, as well as voltage and frequency support for AC and DC buses, can be obtained using this control scheme. It successfully enhances the system's anti-interference properties while lessening the effects of abrupt changes in load disturbances and enhancing the HMG's stability.

This paper proposes a BIC control strategy based on π-VSG with the following main contributions:

(1) Innovative power allocation and bi-directional flow realization: The bi-directional power flow between subgrids is successfully realized by implementing virtual resistors for power sharing and

allocation. Compared with other control techniques, this method only changes the external control loop of the converter without mode switching, which reduces the power loss and instability factors and effectively solves the deficiencies of the traditional control strategy in terms of the flexibility and stability of power allocation.

(2) Comprehensive voltage and frequency support and inertia provision: The proposed strategy can provide voltage and frequency support for the AC and DC buses and inertia for the AC and DC subgrids. This feature enables the AC/DC subgrid to share the disturbance effects by adjusting the virtual capacitance during sudden load changes, which improves the situation in which the traditional control strategy cannot consider the dynamic performance of both sides simultaneously.

(3) Improved dynamic response and anti-disturbance performance: Under load fluctuation, the π-VSG control effectively enhances the anti-disturbance of the AC frequency and DC voltage in the HMG system, improves system stability, meets the power-sharing control objective between the AC and DC subgrids, and overcomes the problem of the traditional control strategy's poor dynamic response to load change.

To confirm the efficacy of this control approach, a standard HMG system was built using PSCAD/EMTDC simulation software for this research.

2 π-VSG Control

This paper mainly discusses the BIC control of HMG in island mode. Fig. 1 shows the structure of AC-DC HMG. In the HMG, the offsets of AC frequency and DC bus voltage are the main metrics reflecting the amount of active power inequality in AC and DC MGs, respectively.

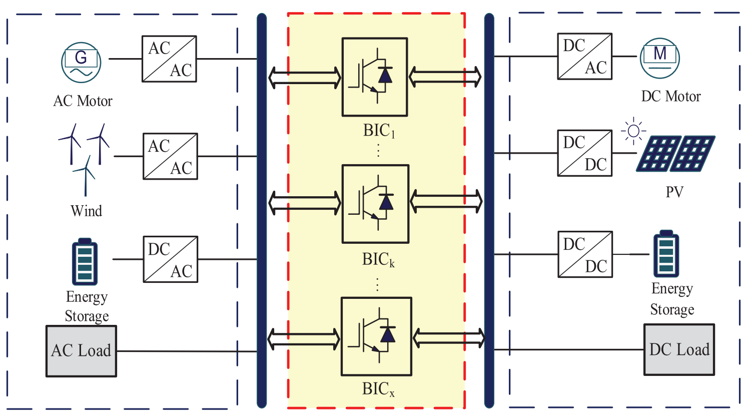

Figure 1: Structure diagram of HMG

Droop control has been used in both AC and DC MGs to balance the distribution of AC and DC active loads [21]. Traditional droop control enables power sharing and provides voltage and frequency support in HMGs, but it suffers from fast response and lack of inertia [22]. Virtual resistors and inductors have been proposed in the literature [20] for power distribution and inertia control via BIC-based generalized DC motor electromotive force (G-DCEMF) control. In Fig. 2, the G-DCEMF control model is displayed.

The G-DCEMF control equations are as follows:

$$\Delta U_{dc} = R_a \Delta I + L_a \frac{d\Delta I}{dt} + K_\omega \Delta\omega \tag{1}$$

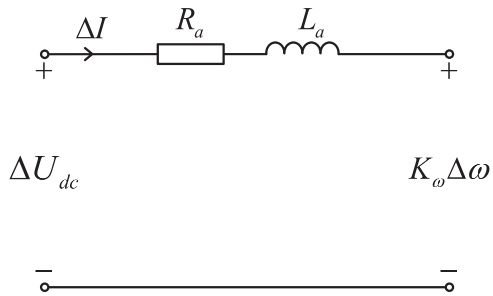

Figure 2: G-DCEMF control model

where R_a is the virtual resistance, K_ω is the electromotive force coefficient, ΔU_{dc} is the DC voltage deviation, $\Delta\omega$ is the AC frequency deviation, and ΔI is the deviation of the current flowing through the BIC.

Neglecting the virtual inductance L_a, the power-sharing of the G-DCEMF control for the BIC can be expressed as

$$\Delta U = R_a \Delta I + K_\omega \Delta\omega \tag{2}$$

In (2), K_ω can be determined by

$$K_\omega = \frac{M_u}{M_\omega} \tag{3}$$

The values of M_u and M_ω represent the permissible ranges for fluctuations in U_{dc} and ω, respectively.

The active power reference value P_{ref} of BIC can be obtained by

$$P_{ref} = (U_{dcN} + \Delta U_{dc})(I_0 + \Delta I_{bic}) \approx U_{dcN} \frac{\Delta U_{dc} - K_\omega \Delta\omega}{R_a} \tag{4}$$

In the proposed G-DCEMF control, S_N should be expressed as

$$S_N = \left|P_{ref}\right|_{\max} = U_{dcN} \frac{M_u + K_\omega M_\omega}{R_a} \tag{5}$$

As a result, the BIC's virtual resistance R_a can be calculated using

$$R_a = U_{dcN} \frac{2M_u}{S_N} = U_{dcN} \frac{2K_\omega M_\omega}{S_N} \tag{6}$$

Virtual capacitors are more suitable for voltage-based control, while virtual inductors used in G-DCEMF control are more suitable for current-based control. To realize sufficient voltage and frequency support for the HMG during islanding operation, virtual inductance in the G-DCEMF is converted to virtual capacitance, thus proposing π-VSG control.

2.1 Active Power Loop Control of BIC

The mechanical motion equation of VSG is shown in (7).

$$J\omega\frac{d\omega}{dt} = P_m - P_e \tag{7}$$

where J is moment of inertia, P_m is mechanical power, and P_e is electromagnetic power.

For better integration with the G-DCEMF control, Eq. (7) can be transformed into

$$C_\omega\frac{dU_\omega}{dt} = \frac{P_m - P_e}{U_\omega} = I_m - I_e \tag{8}$$

where

$$\begin{aligned} U_\omega &= K_\omega\omega \\ C_\omega &= J/K_\omega^2 \end{aligned} \tag{9}$$

where U_ω is the virtual voltage of the AC frequency converted to the DC side, and C_ω is the virtual capacitor on the AC side.

In traditional VSG control, the dynamic response of AC frequency is considered, but the oscillation of DC voltage has not been considered. Consequently, a DC voltage control mode similar to (8) is proposed as

$$C_u\frac{dU_{dc}}{dt} = I_{in} - I_{out} \tag{10}$$

where C_u is the virtual capacitor on the DC side.

Likewise, taking into account the governing equation's initial state, a π-VSG control model applied to BIC is proposed based on (2), (8), and (10), as shown in Fig. 3.

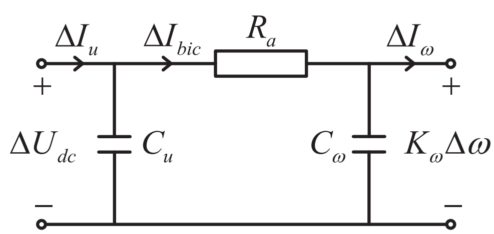

Figure 3: BIC π-VSG control model

Based on Fig. 3, Eq. (11) can be obtained.

$$\begin{aligned} \Delta U_{dc} &= R_a\Delta I_{bic} + \Delta U_\omega \\ C_u\frac{d\Delta U_{dc}}{dt} &= \Delta I_u - \Delta I_{bic} \\ C_\omega\frac{d\Delta U_\omega}{dt} &= \Delta I_{bic} - \Delta I_\omega \end{aligned} \tag{11}$$

where

$$\Delta U_\omega = K_\omega\Delta\omega$$

$$\Delta I_u \approx \Delta I_\omega \approx \frac{\Delta P_{bic}}{U_{dcN}} = \frac{P_{bic} - P_0}{U_{dcN}} \tag{12}$$

Combining (11) and (12), Eq. (13) can be obtained via Laplace transform.

$$\frac{C_\omega}{2} s\Delta U_\omega - \frac{C_u}{2} s\Delta U_{dc} = \frac{\Delta U_{dc} - \Delta U_\omega}{R_a} - \frac{\Delta P_{bic}}{U_{dcN}} \tag{13}$$

The BIC transmission power is expressed as Eq. (14), which consists of a steady state component and a transient component. The transient component is the actively transmitted inertial power ΔP_{vir}. The frequency will fall below the rate when there is a sudden rise in the AC load without an additional power supply. To give the AC frequency priority support, the BIC sends the inertial power ΔP_{vir} to the AC subgrid. When the DC load grows significantly and no more power input is available, the BIC transfers inertial power ΔP_{vir} to the DC subgrid to offer prioritised DC voltage support.

$$\begin{aligned} P_{bic} &= U_{dcN} \left(\underbrace{\frac{\Delta U_{dc} - \Delta U_\omega}{R_a}}_{\text{steady-state component}} + \underbrace{\frac{C_u}{2} s\Delta U_{dc} - \frac{C_\omega}{2} s\Delta U_\omega}_{\text{transient component}} \right) \\ \Delta P_{vir} &= U_{dcN} \left(\frac{C_u}{2} s\Delta U_{dc} - \frac{C_\omega}{2} s\Delta U_\omega \right) \end{aligned} \tag{14}$$

And because

$$\omega = s\theta \tag{15}$$

where θ is the phase angle.

The control block diagram of the active loop of BIC can be obtained, as shown in Fig. 4.

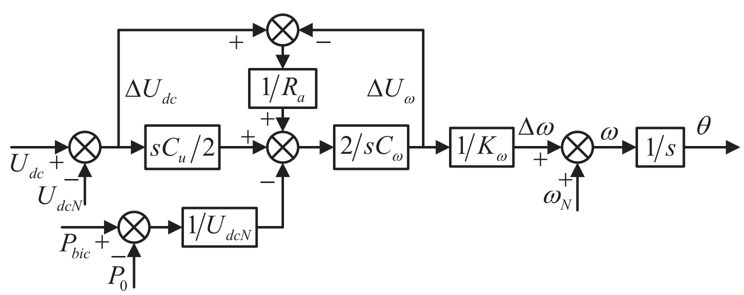

Figure 4: BIC π-VSG active loop control model

2.2 Reactive Power Loop Control of BIC

The reactive power loop of the BIC adopts reactive power-voltage (Q-V) droop control, and Eq. (16) is the excitation control of VSG.

$$E_m = \frac{1}{sK_Q} \left[D_q (V_n - V) + (Q_0 - Q_{bic}) \right] \tag{16}$$

where E_m is the AC voltage amplitude reference value, K_Q is the reactive inertia coefficient, D_q is the droop coefficient of Q-V control, V_n and V are the AC voltage amplitude and actual values, respectively, and Q_0 and Q_{bic} are the BIC reactive power initial and actual values, respectively.

The frequency and phase signal output by the active loop and the voltage amplitude signal output by the reactive loop can be synthesized into the reference voltage e_{abc} by

$$\begin{cases} e_a = E_m \sin\theta \\ e_b = E_m \sin(\theta - 2\pi/3) \\ e_c = E_m (\sin\theta + 2\pi/3) \end{cases} \tag{17}$$

2.3 Voltage and Current Double Closed-Loop Control of BIC

Fig. 5 is the voltage-current double closed-loop control diagram. When the BIC needs to ensure the stability of the HMG, the actual value of the BIC power transmission and the DC side bus voltage are synthesized to obtain the voltage reference value after passing through the π-VSG control link together. After the voltage-current loop and SPWM control, the switching signal is obtained to realize the stabilization and control of the voltage and frequency of the HMG.

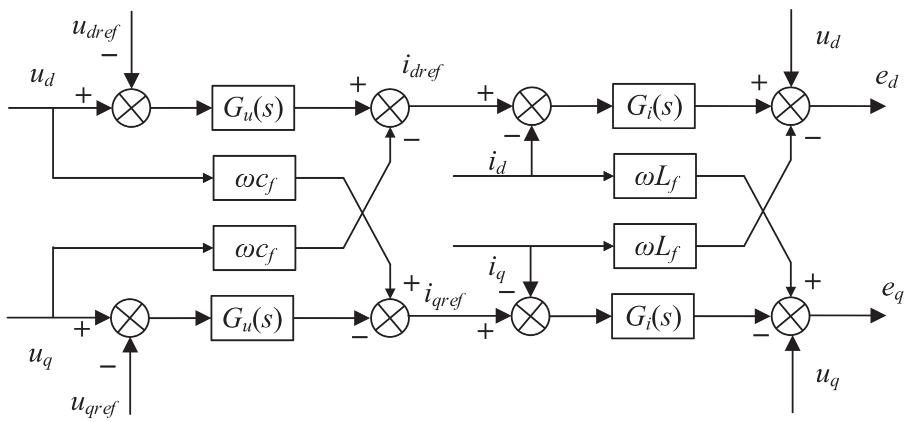

Figure 5: Voltage and current double closed-loop control model

The primary circuit, the π-VSG control, and the voltage-current double closed-loop control together form the overall π-VSG control model of the BIC. Fig. 6 is the π-VSG overall control block diagram of BIC in HMG.

3 Stability Analysis

For the proposed π-VSG control, a small signal model is established, and the dynamic responses of the AC frequency and DC voltage as the load power varies are determined. Below is the active power loop small signal model analysis with a single BIC.

3.1 Small Signal Analysis

In the closed-loop control system of the BIC, the underlying voltage-current dual closed-loop control responds very rapidly with negligible response time compared to the response time of the π-VSG control. Therefore, only the real-time tracking performance of the voltage-current double closed-loop on the voltage and current reference values are considered in the small-signal modelling, as shown in Fig. 5, the BIC takes u_{dref} and u_{qref}. As input, and finally realizes the control of converter output voltage u_d and u_q. That is, $u_d = u_{dref}$ and $u_q = u_{qref}$ always hold during fast tracking, so the transfer function of the voltage-current double-closed loop can be viewed as a constant 1.

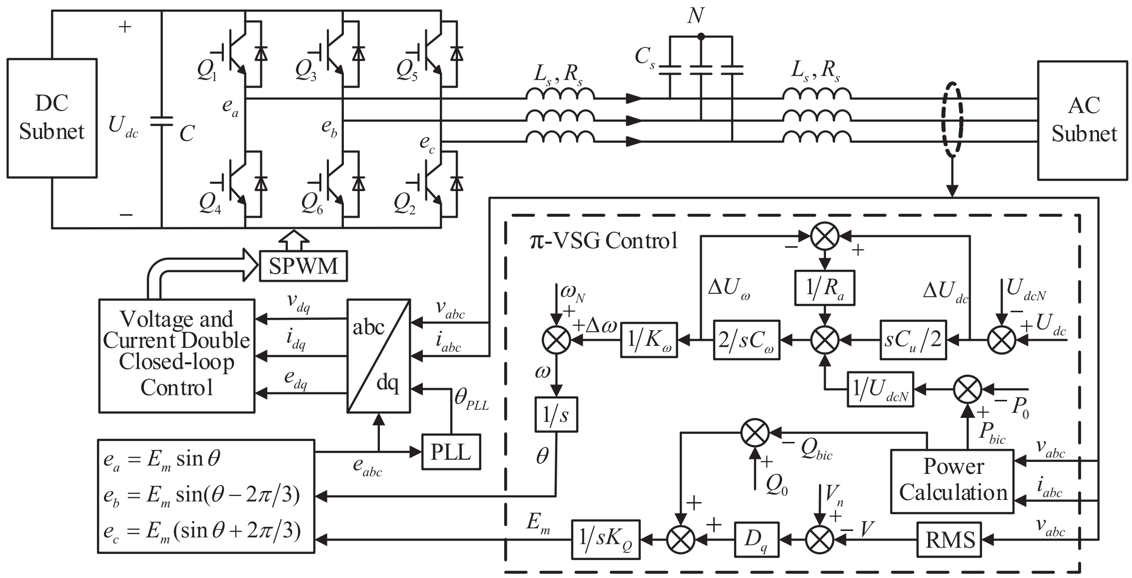

Figure 6: BIC π-VSG overall control model

The BIC is comparable to a voltage source in series with an output impedance, whose reactance value is generally much greater than the resistance value. Thus, the BIC's active power output may be expressed as

$$P_{bic} = \frac{3EU}{X}\sin\delta = K_{P\delta}\sin\delta \tag{18}$$

where $K_{P\delta}$ is a constant coefficient, U is the output voltage amplitude, E is the amplitude of the output electromotive force of BIC, X is BIC equivalent output impedance, and δ, be expressed by (19), is the phase difference between the output electromotive force and the output voltage.

$$\delta = \int \left(\omega - \omega_g\right) dt \tag{19}$$

where ω_g is the angular frequency of the output voltage.

The small signal model is formulated based on (13), (18), and (19) and eliminates the steady-state quantity. Due to $\sin\delta \approx \delta$ and $\cos\delta \approx 1$, the small signal model can be gotten as

$$\begin{aligned}
&\frac{C_\omega}{2}sK_\omega\left(\hat{\omega} - \hat{\omega}_N\right) - \frac{C_u}{2}s\left(\hat{U}_{dc} - \hat{U}_{dcN}\right) \\
&= \frac{\left(\hat{U}_{dc} - \hat{U}_{dcN}\right) - K_\omega\left(\hat{\omega} - \hat{\omega}_N\right)}{R_a} - \frac{\hat{P}_{bic} - \hat{P}_0}{U_{dcN}} \\
&\hat{P}_{bic} = K_{P\delta}\hat{\delta} \\
&\hat{\omega} - \hat{\omega}_g = s\hat{\delta}
\end{aligned} \tag{20}$$

In the DC subgrid, ignoring the small signal disturbance of the DC load, Eq. (21) can be obtained as

$$\hat{P}_{bic} = -k_{dc}\hat{U}_{dc} \tag{21}$$

where k_{dc} is the P-U droop coefficient of the DC subgrid.

According to (20) and (21), the active loop small signal model of BIC π-VSG control can be derived, as shown in Fig. 7.

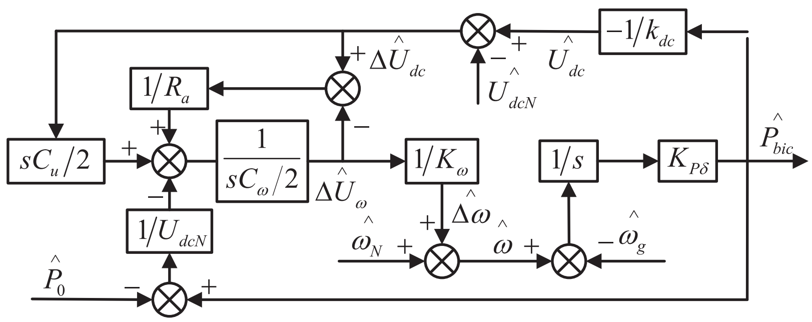

Figure 7: Active loop small signal model of BIC π-VSG control

In the small signal model, the small signal disturbances of U_{dcN}, ω_N and ω_g can be set to 0, and then the closed-loop transfer function of active power can be obtained as

$$\frac{\hat{P}_{bic}(s)}{\hat{P}_0(s)} = \frac{\dfrac{k_{dc}}{U_{dcN}}}{\dfrac{C_\omega K_\omega k_{dc}}{2K_{P\delta}}s^2 + \left(\dfrac{C_u}{2} + \dfrac{K_\omega k_{dc}}{R_a K_{P\delta}}\right)s + \left(\dfrac{1}{R_a} + \dfrac{k_{dc}}{U_{dcN}}\right)} \tag{22}$$

Assuming the denominator is zero, Eq. (22) can be transformed into

$$C_u\frac{\dfrac{1}{2}s}{\dfrac{C_\omega K_\omega k_{dc}}{2K_{P\delta}}s^2 + \dfrac{K_\omega k_{dc}}{R_a K_{P\delta}}s + \dfrac{1}{R_a} + \dfrac{k_{dc}}{U_{dcN}}} = -1 \tag{23}$$

The left side of (18) can be regarded as the equivalent open-loop transfer function, where C_u is the root locus gain. When $1/C_\omega$ ranges from 0 to infinity, the pole distribution of the equivalent open-loop transfer function on the s plane is displayed in Fig. 8. It is clear that regardless of the value of C_ω, the pole of the open-loop transfer function is always on the left half axis of the s plane. Beginning at the pole of the open-loop transfer function and ending at zero is the root locus of the closed-loop transfer function. There is a root locus that ends at negative infinity since the equivalent open-loop transfer function has two poles and one zero with a value of 0. In the s plane, the pole distribution of the C_u closed-loop transfer function from 0 to infinity is displayed in Fig. 9 for C_ω values of 0.1, 1, and 10. So, in the π-VSG control strategy's small signal model, the closed-loop root locus of active power is always in the left half plane, regardless of the values of C_ω and C_u. This suggests that the control system is always stable under small disturbances and that variations in C_u and C_ω only impact the small signal system's damping state.

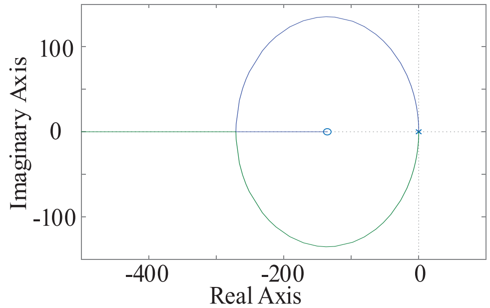

Figure 8: The pole distribution of the equivalent open-loop transfer function on the s plane

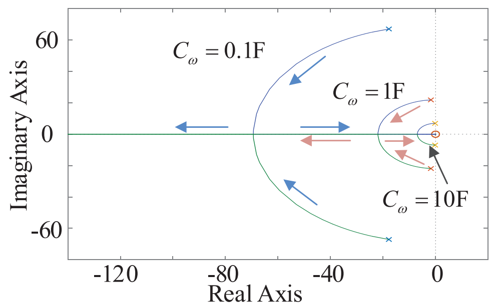

Figure 9: The pole distribution of the closed-loop transfer function on the s plane

3.2 Dynamic Response of AC Frequency and DC Voltage

In HMG, the load power variation ΔP_L satisfies (24).

$$\Delta P_L = -k_{ac}\Delta\omega_{ac\_L} - k_{dc}\Delta U_{dc\_L} \tag{24}$$

where k_{ac} is the P-ω droop coefficient of the AC subgrid, $\Delta\omega_{ac\_L}$ and ΔU_{dc_L} are AC frequency variation and DC voltage variation caused by ΔP_L, respectively.

The load power variation in the AC subgrid ΔP_{Lac} satisfies (25).

$$\begin{aligned}\Delta P_{Lac} &= -k_{ac}\Delta\omega_{ac\_Lac} + \Delta P_{bic\_Lac}\\ &= -k_{ac}\Delta\omega_{ac\_Lac} - k_{dc}\Delta U_{dc\_Lac}\end{aligned} \tag{25}$$

where ΔP_{i_Lac} is the BIC power variation caused by ΔP_{Lac}.

In combination with (13) and (25), the AC frequency variation $\Delta\omega_{ac\_Lac}$ and the DC voltage variation ΔU_{dc_Lac} caused by ΔP_{Lac} can be expressed as

$$\begin{aligned}\Delta\omega_{ac\_Lac} &= -\frac{b_{\omega0}s + b_{\omega1} + k_{dc}/U_{dcN}}{a_0 s + a_1}\Delta P_{Lac}\\ \Delta U_{dc\_Lac} &= -\frac{b_{u0}s + b_{u1}}{a_0 s + a_1}\Delta P_{Lac}\end{aligned} \tag{26}$$

where

$$a_0 = (C_u k_{ac} + C_\omega K_\omega k_{dc})/2$$

$$a_1 = (k_{ac} + K_\omega k_{dc})/R_a + k_{ac}k_{dc}/U_{dcN}$$

$$b_{\omega 0} = C_u/2, b_{\omega 1} = 1/R_a$$
$$b_{u0} = C_\omega K_\omega/2, b_{u1} = K_\omega/R_a \tag{27}$$

Similarly, the load power variation in the DC subgrid ΔP_{Ldc} satisfies (28).

$$\begin{aligned}\Delta P_{Ldc} &= -\Delta P_{bic\_Ldc} - k_{dc}\Delta U_{dc\_Ldc} \\ &= -k_{ac}\Delta\omega_{ac\_Ldc} - k_{dc}\Delta U_{dc\_Ldc}\end{aligned} \tag{28}$$

where ΔP_{bic_Ldc} is the BIC power variation caused by ΔP_{Ldc}.

Hence, the AC frequency variation $\Delta\omega_{ac\_Ldc}$ and DC voltage variation ΔU_{dc_Ldc} caused by ΔP_{Ldc} are

$$\Delta\omega_{ac\_Ldc} = -\frac{b_{\omega 0}s + b_{\omega 1}}{a_0 s + a_1}\Delta P_{Ldc}$$
$$\Delta U_{dc\_Ldc} = -\frac{b_{u0}s + b_{u1} + k_{ac}/U_{dcN}}{a_0 s + a_1}\Delta P_{Ldc} \tag{29}$$

As shown, the values of C_ω and C_u only influence the dynamic response, but the value of R_a influences the steady-state values of AC frequency and DC voltage, which are established by (6).

Ignoring the different terms between (26) and (29), the analysis can be simplified to

$$\Delta\omega_{ac\_L} = -\left(\frac{b_{\omega 0}}{a_0} + \frac{-a_1 b_{\omega 0}/a_0 + b_{\omega 1}}{a_0 s + a_1}\right)\Delta P_L$$
$$\Delta U_{dc\_L} = -\left(\frac{b_{u0}}{a_0} + \frac{-a_1 b_{u0}/a_0 + b_{u1}}{a_0 s + a_1}\right)\Delta P_L \tag{30}$$

It is evident from (30) that in the event of a sudden change in the load power, both the AC frequency and the DC voltage will likewise change quickly. However, these changes will eventually recover to the new steady-state operation point. The increase of C_u will lead to the rise of $b_{\omega 0}/a_0$ and the decrease of b_{u0}/a_0, which means that the sudden change of AC frequency will increase and the sudden change of DC voltage will decrease. When C_ω increases, the AC frequency mutation decreases, and the DC voltage mutation increases. When C_u is 0, the AC frequency will change slowly, similar to the traditional VSG control. However, the sudden change of DC voltage reaches the maximum, which means that the DC bus voltage entirely bears the impact of the load power fluctuation. The proposed π-VSG control can make AC frequency and DC voltage jointly withstand load disruptions. The whole HMG will react when a load disturbance occurs in a single subgrid, enhancing that subgrid's anti-interference capabilities.

According to Fig. 7, the closed-loop transfer function between $\Delta\omega$ and P_{bic} can be obtained.

$$\frac{\Delta\omega}{P_{bic}} = \frac{2K_{P\delta}s}{U_{dcN}C_\omega K_\omega s^2 + (2U_{dcN}K_\omega/R_a)\,s + 1} \tag{31}$$

According to Fig. 7, the closed-loop transfer function between ΔU_{dc} and P_{bic} can be obtained.

$$\frac{\Delta U_{dc}}{P_{bic}} = \frac{-\dfrac{1}{U_{dcN}}}{\dfrac{C_\omega K_\omega k_{dc}}{2K_{P\delta}}s^2 + \left(\dfrac{C_u}{2} + \dfrac{K_\omega k_{dc}}{R_a K_{P\delta}}\right)s + \left(\dfrac{1}{R_a} + \dfrac{k_{dc}}{U_{dcN}}\right)} \tag{32}$$

Fig. 10 gives the output power step response curves caused by the change of virtual capacitance on the AC and DC sides. As shown in Fig. 10a, when the virtual capacitance C_u on the DC side is kept constant, as C_ω increases, it will bring some inertia to the system, but at the cost of an increase in the system's overshoot; Fig. 10b shows that, by fixing the value of the virtual capacitance C_ω on the AC side, the DC voltage overshoot will decrease as C_u increases, and at the same time accelerates the system back to a steady state.

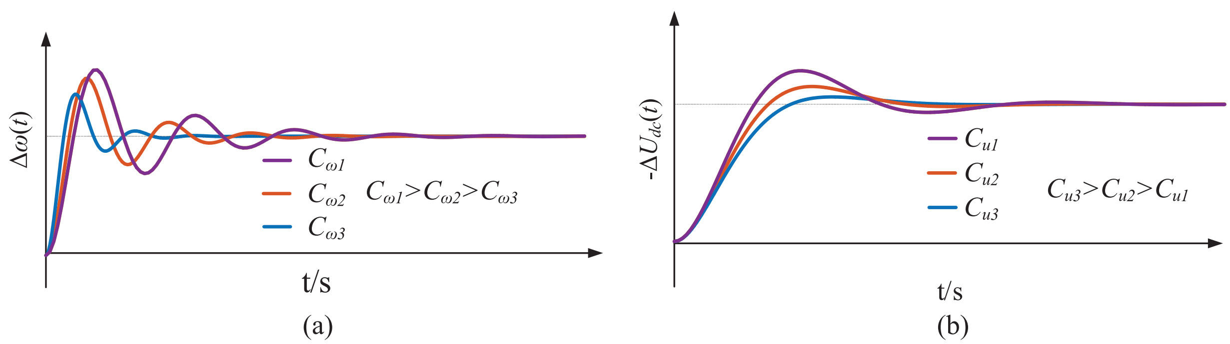

Figure 10: Step response curve of output power P_{bic} varying with control parameters

Furthermore, $M_{\omega 0}$ and M_{u0} are the maximum allowable fluctuation ranges of U_{dc} and ω, respectively. The inequalities between C_u and C_ω should be

$$\begin{aligned} &\frac{b_{\omega 0}}{a_0}\Delta P_L \le \frac{b_{\omega 0}}{a_0}k_{ac}M_\omega \le M_{\omega 0} \\ &\frac{b_{u0}}{a_0}\Delta P_L \le \frac{b_{u0}}{a_0}k_{dc}M_u \le M_{u0} \end{aligned} \tag{33}$$

If both AC frequency and DC voltage change rate must satisfy the conditions listed in (34) correspondingly.

$$\begin{aligned} &\left|\frac{d\omega_{ac}}{dt}\right| \le M_\omega' \\ &\left|\frac{dU_{dc}}{dt}\right| \le M_u' \end{aligned} \tag{34}$$

where M_ω' and M_u' are the maximum AC frequency and DC voltage change rate values, respectively.

Then, the values of C_u and C_ω should also meet (35).

$$\begin{aligned}
\left.\frac{d\left|\Delta U_{dc}\right|}{dt}\right|_{t=0} &= \frac{a_1}{a_0}\left|-\frac{b_{u0}}{a_0}+\frac{b_{u1}}{a_1}\right|\Delta P_L \\
&\le \frac{\left|a_0 b_{u1}-a_1 b_{u0}\right|}{a_0^2}k_{dc}M_u \le M_u' \\
\left.\frac{d\left|\Delta\omega_{ac}\right|}{dt}\right|_{t=0} &= \frac{a_1}{a_0}\left|-\frac{b_{\omega 0}}{a_0}+\frac{b_{\omega 1}}{a_1}\right|\Delta P_L \\
&\le \frac{\left|a_0 b_{\omega 1}-a_1 b_{\omega 0}\right|}{a_0^2}k_{ac}M_\omega \le M_\omega'
\end{aligned} \tag{35}$$

It can be seen from the previous analysis that the values of C_u and C_ω not only provide inertia for the system but also affect the sudden change of AC frequency and DC voltage caused by ΔP_L. The increase in C_u will lead to the sudden growth of the abrupt value of AC frequency and the sudden decrease of the abrupt value of DC voltage. The increase in C_ω will lead to the sudden decrease of the abrupt value of AC frequency and the sudden increase of DC voltage. In general, the sudden change of DC bus voltage often has less impact on the subgrid than that of AC bus frequency.

4 Simulation Results

To test the efficacy of π-VSG control, an AC/DC HMG simulation model for island operation is constructed using PSCAD/EMTDC simulation software. Fig. 6 displays the BIC control model, and the DC and AC subgrids use P-U and P-ω droop control, respectively. The simulation parameters are listed in Table 2.

Table 2: System parameters

Parameters	Values
AC line voltage rating (V_N)	0.38 kV
AC frequency rating (f_N)	50 Hz
DC voltage rating (U_{dcN})	0.75 kV
AC subgrid droop coefficient (k_{ac})	0.064 MW/(rad/s)
DC subgrid droop coefficient (k_{dc})	2.67 MW/kV
Range of AC frequency fluctuations (M_ω)	0.5 rad/s
Range of DC voltage fluctuation (M_u)	0.075 kV
Electromotive force coefficient (K_ω)	0.024
BIC initial active power (P_0)	0 MW
BIC initial reactive power (Q_0)	0 MVar
Rated capacity of the BIC (S_N)	0.5 MW
Virtual resistance (R_a)	0.225 Ω
Virtual capacitance (C_u)	0.3 F
Virtual inductance (C_ω)	1 F

According to the former analysis, when $C_u = 0$ and $C_\omega = 0$, the BIC is under bidirectional droop control. Therefore, to compare different control modes more intuitively and keep other parameters unchanged in this paper, bidirectional droop control is simulated by setting C_u and C_ω to 0. In the proposed π-VSG control, C_u is set to 0.3F, and C_ω is set to 1F.

1) Inverter mode

At t = 2 s, the AC-side load increases by 100 kW; at t = 4 s, the AC-side load decreases by 100 kW. Fig. 11 shows the AC load change simulation diagrams containing the DC voltage, AC frequency, and transmitted active power, as well as the transmitted virtual inertia power waveforms under the bidirectional droop control and the π-VSG control. The blue line indicates that the bidirectional droop control strategy lacks inertia, has no inertial power transfer, responds quickly, and immediately affects the DC-side voltage with significant sudden changes. The red line represents the π-VSG control strategy, which increases the AC frequency and DC voltage inertia and actively transmits the inertial power ΔP_{vir} during the abrupt load change. This is achieved by introducing the virtual parameters C_ω and C_u, which improve the dynamic response characteristics of the AC and DC sides. Fig. 11 shows that the system's steady-state values are the same for both controls, indicating that the π-VSG control exhibits the droop characteristic when it reaches the steady state. However, compared to the bidirectional droop control, the π-VSG control has minor AC frequency and DC voltage fluctuations, and the response is slower with the inertia. Combined with Table 3, it can be seen that the π-VSG control suppresses the overshooting of power, voltage and frequency and actively transfers the inertial power. This means that sudden large fluctuations in power can be avoided during system operation. Meanwhile, its power adjustment time increase possesses corresponding inertia, and the adjustment process is smooth. It does not cause system oscillation or instability, providing a reliable power conversion process.

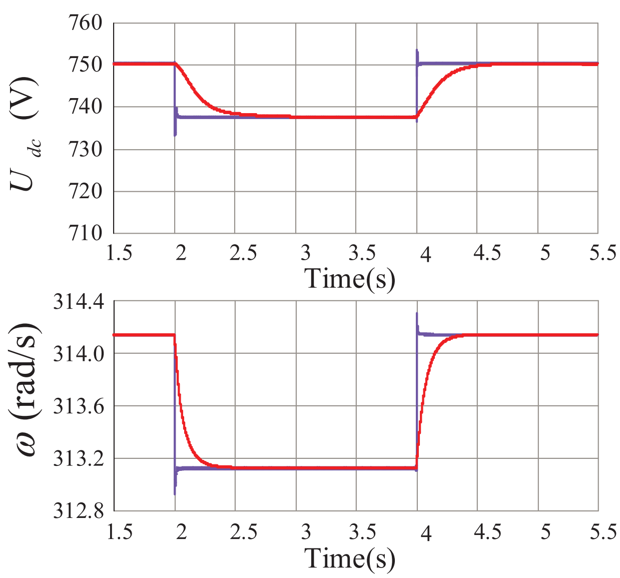

Figure 11: (Continued)

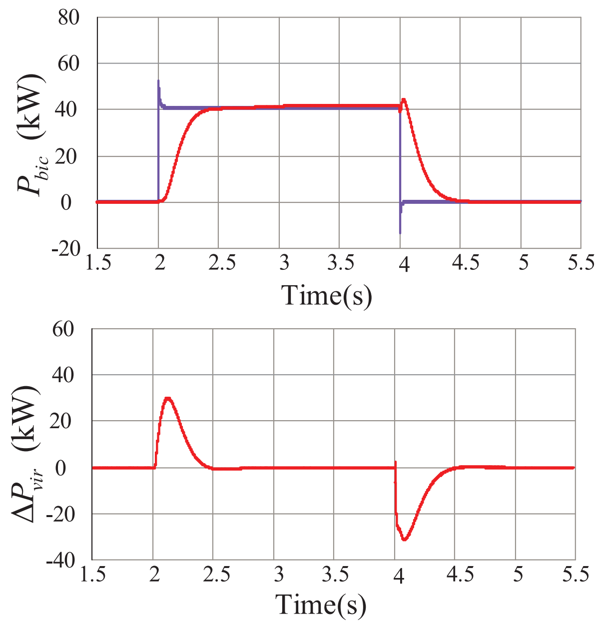

Figure 11: DC bus voltage, BIC active power, AC bus angular frequency waveforms, and virtual inertia power waveforms transferred between subgrids when 100 kW AC load input to the AC subgrid

Table 3: Performance comparison of main parameters in inverter mode

Control strategy	Power overshoot	Power adjustment time	Frequency overshoot	Frequency adjustment time	Voltage overshoot	Voltage adjustment time
Traditional droop control	31.8%	0.05 s	0.13%	0.02 s	0.68%	0.03 s
π-VSG control	0%	0.4 s	0%	0.4 s	0%	0.5 s

2) Rectifier mode

Similarly, at t = 2 s, the DC-side load increases by 100 kW; at t = 4 s, the DC-side load decreases by 100 kW. Fig. 12 shows the DC load change simulation diagrams containing the DC voltage, AC frequency, and transmitted active power, as well as the transmitted virtual inertia power waveforms under the bi-directional droop control and π-VSG control. The maximum fluctuation of AC frequency and DC voltage is about 1 rad/s and 20 V during the dynamic process under bidirectional droop control. However, when using the π-VSG control, the voltage and frequency adjust dynamically throughout 0.4 and 0.3 s to reach a new steady state, which is slower than the dynamic response of bidirectional droop control. The AC frequency gradually decreases in the dynamic process, and the fluctuation in the dynamic process is smaller than using bidirectional droop control. The inverter and rectifier simulations show that when the BIC is controlled with π-VSG, the whole HMG can still distribute the power shortfall of any subgrid. Combined with Table 4, it can be seen that the π-VSG control in the rectifier mode can still suppress the power, voltage and frequency overshoots, actively transfer the inertia power, and fully utilize the potential of the BIC to stabilize the HMG system.

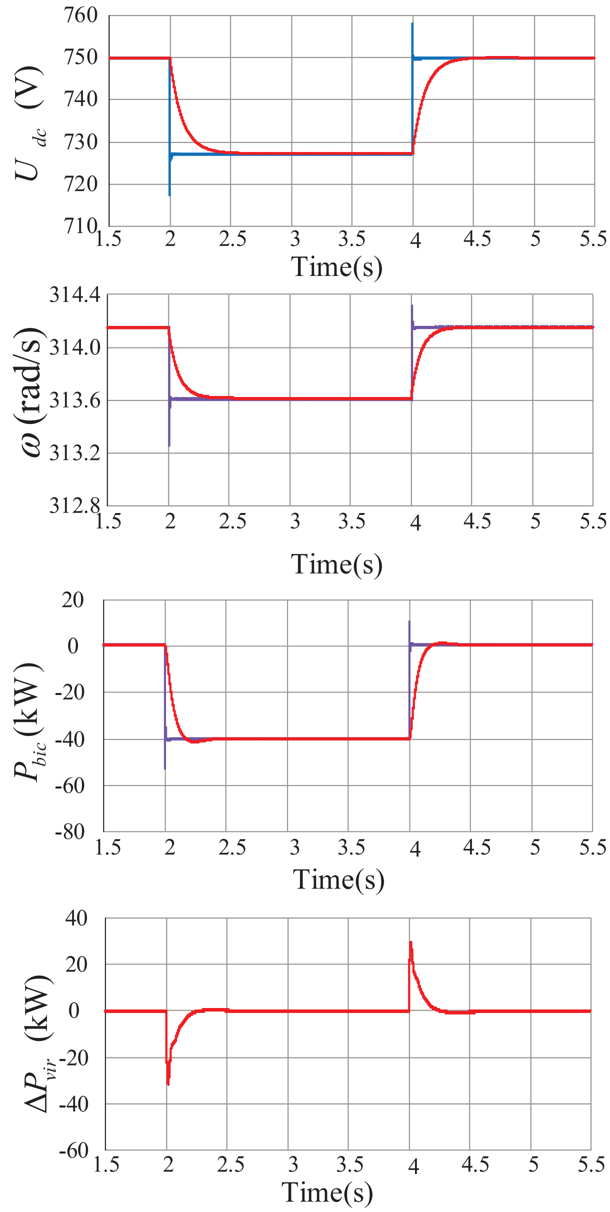

Figure 12: DC bus voltage, BIC active power, AC bus angular frequency waveforms, and virtual inertia power waveforms transferred between subgrids when 100 kW DC load input to the DC subgrid

Table 4: Performance comparison of main parameters in rectification mode

Control strategy	Power overshoot	Power adjustment time	Frequency overshoot	Frequency adjustment time	Voltage overshoot	Voltage adjustment time
Traditional droop control	32%	0.05 s	0.11%	0.02 s	1.39%	0.03 s
π-VSG control	4.7%	0.4 s	0%	0.3 s	0%	0.4 s

3) Mode transition

At t = 2 s, a DC load of 50 kW is input to the DC subgrid. At t = 3 s, a 100 kW AC load is input to the AC subgrid. At 2∼3 s, the BIC operates in rectifier mode, and the HMG shares the sudden DC load disturbance through the BIC. At 3∼4.5 s, the AC subgrid is heavily loaded, and the BIC operates in inverter mode. The improvement in AC frequency and DC voltage inertia can also be realized during the mode-switching process. At t = 4.5 s, the AC and DC loads are removed, and after about 0.5 s, the system returns to the rated state, and the power transfer is 0. According to Fig. 13, it can be seen that the BIC can flexibly adjust the operation mode according to the changes of HMG measured loads to satisfy the requirement of the BIC's power bidirectional transfer.

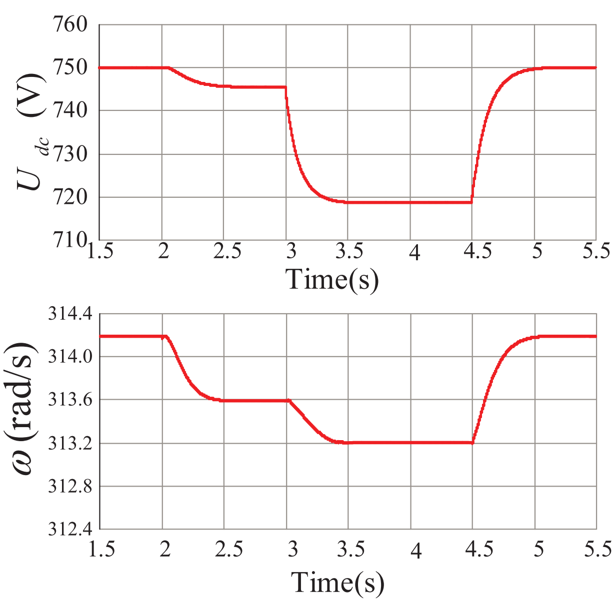

Figure 13: (Continued)

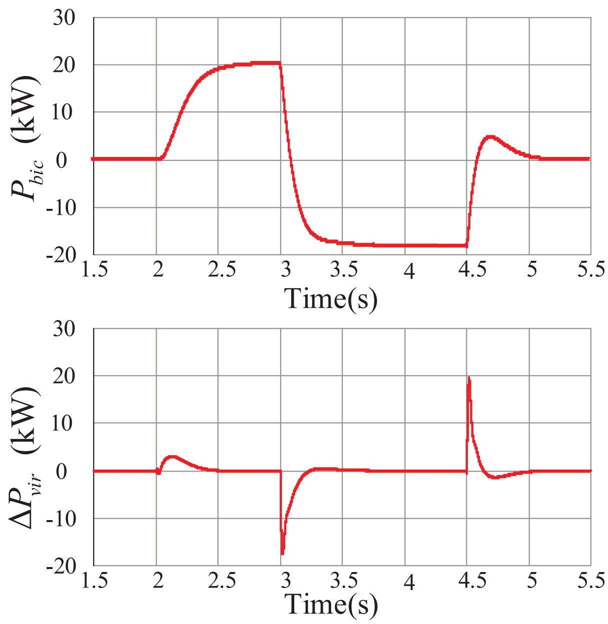

Figure 13: BIC mode transition simulation diagram

4) Power distribution

Meanwhile, to verify the power distribution ability of bidirectional virtual inertia augmentation control, it is known that the power transfer of BIC is related to virtual resistance. Setting the virtual resistance value ratio as R_1:R_2:R_3 = 1:2:3, a 100 kW DC load is put in at t = 2 s to verify the power waveforms at different virtual resistance values. Set the ratio of virtual resistance values as R_1:R_2:R_3 = 1:2:3, and at t = 2 s, put in 100 kW AC load to verify the power waveforms at different virtual resistance values. From Fig. 14, the BIC transmission power ratio is 3:2:1, and a flexible proportional transmission power distribution is realized.

In summary, the proposed BIC π-VSG control can provide inertia for HMG to reduce the impact of sudden load changes on the system's stable operation. The virtual resistors enable flexible power distribution for BICs. The virtual inertia parameters C_ω and C_u do not influence the steady-state performance and only optimize the transient performance. The transfer of virtual inertial power through BIC provides inertial support for the DC voltage and AC frequency, improving the HMG system's immunity performance.

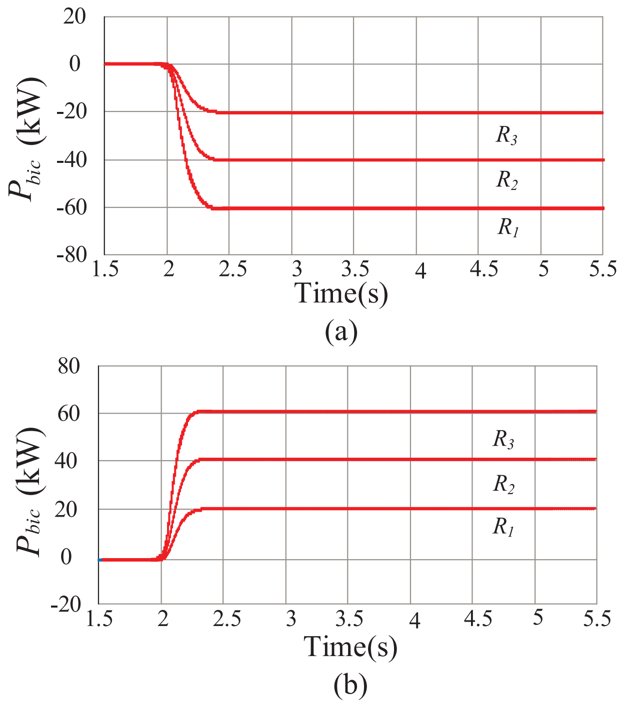

Figure 14: BIC power distribution simulation diagram

5 Conclusion

The transfer of virtual inertia between subgrids is a way to improve the stability of the HMG system by balancing the individual subgrids through BIC control. This approach enables and improves the transient performance on both sides of the system. So, in this paper, the π-VSG control method of BIC in HMG is proposed, and the following conclusions are obtained through example simulations:

(1) BIC's power-sharing can be flexibly controlled by using virtual resistance, which facilitates the optimization of power transfer in the islanded HMG system.

(2) The π-VSG control can actively transfer inertial power to improve the dynamic response of AC frequency and DC voltage and adjust the power flow according to the load fluctuation of AC and DC subgrids, improving immunity and stability compared with the droop control.

(3) The power distribution and dynamic response of the BIC can be adapted to different operating modes. The virtual inertia parameters C_ω and C_u provide inertial support for AC and DC subgrids without affecting the steady-state values of the control system.

Meanwhile, future work and research directions are as follows:

(1) Parameter optimization research: further explore the optimization methods of virtual capacitance C_ω and C_u, virtual resistance R_a to adapt to more complex operating conditions.

(2) Research on parallel operation of multiple machines: for parallel operation of multiple machines, in-depth research on their interaction and coordination control methods to ensure the stability and reliability of the system in large-scale applications.

(3) Combination with other control strategies: Consider combining the π-VSG control strategy with other advanced control technologies (e.g., model predictive control, distributed cooperative control, etc.) to give full play to their respective advantages.

Acknowledgement: None.

Funding Statement: This research was funded by "The Fourth Phase of 2022 Advantage Discipline Engineering-Control Science and Engineering", grant number 4013000063.

Author Contributions: The authors confirm their contribution to the paper as follows: study conception and design: Dongyang Yang; data collection: Kai Shi; analysis and interpretation of results: Dongyang Yang, Kai Shi; draft manuscript preparation: Dongyang Yang. All authors reviewed the results and approved the final version of the manuscript.

Availability of Data and Materials: The authors confirm that the data used in this study are available on request.

Ethics Approval: Not applicable.

Conflicts of Interest: The authors declare no conflicts of interest to report regarding the present study.

References

[1] X. R. Xie, J. B. He, H. Y. Mao, and H. Z. Li, "Discussion on new issues and categorization of "double-high" power system stability," *Chin. J. Electr. Eng.*, vol. 41, no. 10, pp. 461–475, Nov. 2021. doi: 10.13334/j.0258-8013.pcsee.201405.

[2] A. A. Eajal, A. H. Yazdavar, E. F. El-Saadany, and M. M. A. Salama, "Optimizing the droop characteristics of hybrid AC/DC MGs for precise power sharing," *IEEE Syst. J.*, vol. 15, no. 1, pp. 560–569, Mar. 2021. doi: 10.1109/JSYST.2020.2984623.

[3] F. Sayeed *et al.*, "A novel and comprehensive mechanism for the energy management of a hybrid micro-grid system," *Energy Rep.*, vol. 8, no. 5, pp. 847–862, Nov. 2022. doi: 10.1016/j.egyr.2022.09.207.

[4] A. O. Rousis, I. Konstantelos, and G. Strbac, "A planning model for a hybrid AC-DC microgrid using a novel GA/AC OPF algorithm," *IEEE Trans. Power Syst.*, vol. 35, no. 1, pp. 227–237, Jan. 2020. doi: 10.1109/TPWRS.2019.2924137.

[5] Y. Wang, A. O. Rousis, and G. Strbac, "Resilience-driven modeling, operation and assessment for a hybrid AC/DC microgrid," *IEEE Access*, vol. 8, pp. 139756–139770, 2020. doi: 10.1109/ACCESS.2020.3013662.

[6] Z. Liu, S. Miao, W. Wang, and D. Sun, "Comprehensive control scheme for an interlinking converter in a hybrid AC/DC MG," *CSEE J. Power Energy Syst.*, vol. 7, no. 4, pp. 719–729, Jul. 2021. doi: 10.17775/CSEEJPES.2020.00970.

[7] X. Shen, D. Tan, Z. Shuai, and A. Luo, "Control techniques for bidirectional interlinking converters in hybrid microgrids: Leveraging the advantages of both ac and dc," *IEEE Power Electron. Mag.*, vol. 6, no. 3, pp. 39–47, Sep. 2019. doi: 10.1109/MPEL.2019.2925298.

[8] Z. Gao, C. Li, Y. Liu, C. Tian, W. Teng and Y. Rao, "Bidirectional droop control of AC/DC hybrid MG interlinking converter," in *Proc. 2nd Int. Conf. Saf. Produce Inf. (IICSPI)*, 2019, pp. 213–217. doi: 10.1109/IICSPI48186.2019.9095894.

[9] S. Peyghami, H. Mokhtari, and F. Blaabjerg, "Autonomous operation of a hybrid AC/DC MG with multiple interlinking converters," *IEEE Trans. Smart Grid*, vol. 9, no. 6, pp. 6480–6488, Nov. 2018. doi: 10.1109/TSG.2017.2713941.

[10] M. Ahmed, L. Meegahapola, M. Datta, and A. Vahidnia, "A novel hybrid AC/DC microgrid architecture with a central energy storage system," *IEEE Trans. Power Deliv.*, vol. 37, no. 3, pp. 2060–2070, Jun. 2022. doi: 10.1109/TPWRD.2021.3103742.

[11] J. Wang, C. Jin, and P. Wang, "A uniform control strategy for the interlinking converter in hierarchical controlled hybrid AC/DC microgrids," *IEEE Trans. Ind. Electron.*, vol. 65, no. 8, pp. 6188–6197, Aug. 2018. doi: 10.1109/TIE.2017.2784349.

[12] M. Najafzadeh, R. Ahmadiahangar, O. Husev, I. Roasto, T. Jalakas and A. Blinov, "Recent contributions, future prospects and limitations of interlinking converter control in hybrid AC/DC microgrids," *IEEE Access*, vol. 9, pp. 7960–7984, Jan. 2021. doi: 10.1109/ACCESS.2020.3049023.

[13] G. Melath, S. Rangarajan, and V. Agarwal, "A novel control scheme for enhancing the transient performance of an islanded hybrid AC-DC microgrid," *IEEE Trans. Power Electron.*, vol. 34, no. 10, pp. 9644–9654, Oct. 2019. doi: 10.1109/TPEL.2019.2891637.

[14] K. Shi, W. Song, H. Ge, P. Xu, Y. Yang and F. Blaabjerg, "Transient analysis of microgrids with parallel synchronous generators and virtual synchronous generators," *IEEE Trans. Energy Convers.*, vol. 35, no. 1, pp. 95–105, Mar. 2020. doi: 10.1109/TEC.2019.2943888.

[15] K. Shi, Y. Wang, Y. Sun, P. Xu, and F. Gao, "Frequency-coupled impedance modeling of virtual synchronous generators," *IEEE Trans. Power Syst.*, vol. 36, no. 4, pp. 3692–3700, Jul. 2021. doi: 10.1109/TPWRS.2021.3050568.

[16] C. Jin, C. Jia, J. Fu, and S. Wang, "Inertia control and dynamic performance optimization of interlinking converter based on parameter adaptation," in *2022 Asian Conf. Front. Pow. Energy (ACFPE)*, Chengdu, China, 2022, pp. 489–493. doi: 10.1109/ACFPE56003.2022.9952343.

[17] A. Hosseinipour and H. Hojabri, "Virtual inertia control of PV systems for dynamic performance and damping enhancement of DC MGs with constant power loads," *IET Renew. Pow. Generat.*, vol. 12, no. 4, pp. 430–438, Jan. 2018. doi: 10.1049/iet-rpg.2017.0468.

[18] Z. W. Liu, S. H. Miao, Z. H. Fan, J. Y. Liu, and Q. Y. Tu, "lmproved power flow control strategy of the hybrid AC/DC microgrid based on VSM," *IET Generat., Transmiss. Distribut.*, vol. 13, no. 1, pp. 81–91, Dec. 2018. doi: 10.1049/iet-gtd.2018.5839.

[19] J. R. Shi, Y. Li, L. He, Z. Y. Wang, and S. Q. Jiao, "An integrated inertia control method to enhance the dynamic characteristics of AC-DC hybrid microgrid," *J. Electrotechnol.*, vol. 35, no. 2, pp. 337–345, Jan. 2020. doi: 10.19595/j.cnki.1000-6753.tces.181573.

[20] K. Shi, Y. Chen, P. Xu, Y. Sun, M. Liu and X. Wang, "A generalized DC electromotive force control strategy for Bi-directional interface converters in a standalone hybrid microgrid," *IEEE Trans. Energy Convers.*, vol. 38, no. 2, pp. 1155–1165, Jun. 2023. doi: 10.1109/TEC.2022.3229272.

[21] J. Wang, W. Huang, N. Tai, M. Yu, R. Li and Y. Zhang, "A bidirectional virtual inertia control strategy for the interconnected converter of standalone AC/DC hybrid microgrids," *IEEE Trans. Power Syst.*, vol. 39, no. 1, pp. 745–754, Jan. 2024. doi: 10.1109/TPWRS.2023.3246522.

[22] L. He, Y. Li, J. M. Guerrero, and Y. Cao, "A comprehensive inertial control strategy for hybrid AC/DC microgrid with distributed generations," *IEEE Trans. Smart Grid*, vol. 11, no. 2, pp. 1737–1747, Mar. 2020. doi: 10.1109/TSG.2019.2942736.